# Experimental Study of Relaxation Processes for Divalent Cobalt Ions*

WESLEY P. UNRUH† AND J. W. CULVAHOUSE
*Department of Physics and Astronomy, University of Kansas, Lawrence, Kansas*
(Received 10 July 1962)

The nuclear orientation produced for stable $Co^{59}$ nuclei of divalent cobalt ions in the $X$ site of $La_2Zn_3(NO_3)_{12}\cdot 24H_2O$ by saturation of allowed and forbidden transitions between levels of the hyperfine structure in a strong magnetic field has been deduced from measurements of the intensity of allowed transitions while some other transition was saturated. These measurements give more detailed results than just the nuclear orientation; and, when combined with transient measurements, permit one to deduce the values of the many relaxation rates. The relaxation rates depend strongly on the direction of the applied magnetic field but can all be predicted rather accurately by the theory presented in the preceding paper when an appropriate and reasonable choice is made for the four constants left undetermined in that theory. The temperature dependence of the relaxation rates is of the form $1/(aT+bT^9)$ and, below 2.2°K, the direct process dominates. The most striking effects are the extreme importance of the hyperfine relaxation effects, and a perfect Overhauser effect, producing nuclear alignment opposite in sign from that usually anticipated.

## I. INTRODUCTION

DYNAMIC nuclear orientation has been extensively investigated since the original theoretical paper by Overhauser[1] and particularly since the development of new techniques by Feher[2] and Jeffries.[3] Attempts to use these methods for the orientation of radioactive isotopes have met with varying success.[4,5] It seems that dynamic nuclear orientation is better suited in most cases to a detailed study of the spin-spin and spin-lattice relaxation processes than for the production of a known nuclear orientation as a tool for nuclear physics.

If one wishes to use nuclear orientation for the study of relaxation processes, it is better to replace the detection of gamma-ray anisotropy by a paramagnetic resonance spectrometer which can be used to probe the population distributions produced by the saturation of single transitions of a resolved hyperfine structure. The radio-frequency measurements are easier to make and can give a more detailed picture of the population distributions.

We have chosen to work with the cobalt $X$ ion in $La_2Zn_3(NO_3)_{12}\cdot 24H_2O$ [hereafter denoted by $(La-Zn)\cdot(H_2O)$] because the well resolved and nearly isotropic hyperfine structure simplifies the analysis. The nuclear spin of the 100% abundant $Co^{59}$ is 7/2. The presence of eight allowed hyperfine transitions has complicated the analysis of the relaxation processes, but the complexity offers a crucial test of the theory for these processes, which has been described in the preceding paper (hereafter CUB).

In Sec. II, we discuss the nature of the paramagnetic resonance signal expected from the allowed transitions of the hyperfine structure when some other allowed or a forbidden transition is saturated. The experimental apparatus and procedures are discussed in Sec. III, and the experimental results are presented in Sec. IV.

Section V contains an analysis of the data and a comparison of the experimental results with the theory derived by CUB. The four constants in that theory can be assigned reasonable values which reproduce all of the experimental data in a rather convincing manner.

## II. SIMPLE THEORY

For the case of the cobalt $X$ ion in $(La-Zn)\cdot(H_2O)$, the neglect of the anisotropy of the static spin Hamiltonian ($g_{\parallel}=4.37$, $g_{\perp}=4.31$, $A=0.00986$ cm$^{-1}$, $B=0.00948$ cm$^{-1}$) in the calculation of spin-lattice relaxation processes and the radio-frequency matrix elements is an excellent approximation. In our formal discussion we ignore all quadrupole effects. The simplification of the calculation of the relaxation rates in this approximation has been discussed by CUB.

We assume that the paramagnetic ions are so well dispersed that all of the cross relation processes[6] between hyperfine lines are slow compared with the spin-lattice rates for the high-frequency transitions (those in which the electron spin flips). However, we assume that the spin-spin processes are sufficiently fast that a single transition shows an effectively homogeneous behavior so that the entire line may be saturated without hole burning. As the linewidth of the resonances is certainly of an inhomogeneous nature, an effectively homogeneous behavior clearly requires spin-spin interactions which can keep the different spin packets in thermal equilibrium with each other.[7] Our requirements for the spin-spin processes are not incompatable and can be obtained in a certain concentration range which

* This work was supported in part by a grant from the National Science Foundation; helium gas was supplied by the Office of Naval Research.
† National Science Foundation Fellow 1960–61, present address: Bell Telephone Laboratories, Murray Hill, New Jersey.
[1] A. Overhauser, Phys. Rev. **92**, 411 (1953).
[2] G. Feher, Phys. Rev. **103**, 843 (1956).
[3] C. D. Jeffries, Phys. Rev. **106**, 164 (1957).
[4] C. D. Jeffries, in *Progress in Cryogenics*, edited by K. Mendelssohn (Academic Press Inc., New York, 1961), Vol. 3.
[5] E. Ambler, in *Progress in Cryogenics*, edited by K. Mendelssohn (Academic Press Inc., New York, 1960), Vol. 2.
[6] N. Bloembergen, S. Shapiro, P. S. Pershan, and J. O. Artman, Phys. Rev. **114**, 445 (1959).
[7] A. M. Portis, Phys. Rev. **91**, 1071 (1953).

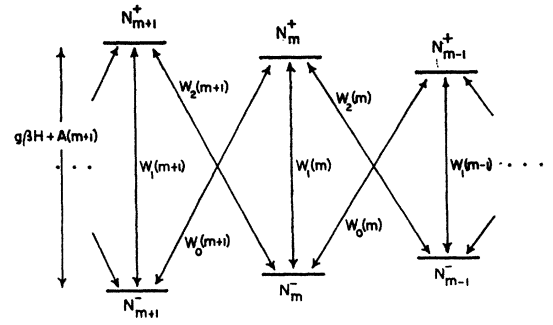


FIG. 1. A schematic diagram of the energy levels of a paramagnetic ion in a strong magnetic field for $A>0$. The level populations are designated and the dominant relaxation processes are shown by arrows.

can be determined by experiment. We also assume, subject to verification, that the allowed and forbidden transitions are so well resolved that they can be saturated separately. For our purposes the spin Hamiltonian for the cobalt ion may be written

$$\mathcal{H}=GS_\zeta+A\mathbf{I}\cdot\mathbf{S}, \tag{1}$$

where $G=g\beta H$ and $\zeta$, the quantization axis, is in the direction of the applied field. For $G\gg A$, the level structure and relaxation processes are depicted in Fig. 1. Our notation for the level population $N_m{}^\pm$ is defined by the figure. The notation used for the relaxation rates in Fig. 1 is the value of the geometric mean of the rates for the processes in which the energy of the spin system increases and decreases. In terms of the notation defined by CUB, Eqs. (27) and (28), they are

$$W_{m\to m-1}{}^+=W_0(m)\alpha^{+1/2}, \tag{2a}$$

$$W_{m-1\to m}{}^-=W_0(m)\alpha^{-1/2}, \tag{2b}$$

$$W_{m\to m}{}^\pm=W_1(m)\alpha^{\pm1/2}, \tag{2c}$$

$$W_{m-1\to m}{}^+=W_2(m)\alpha^{+1/2}, \tag{2d}$$

$$W_{m\to m-1}{}^-=W_2(m)\alpha^{-1/2}, \tag{2e}$$

where $\alpha=\exp(-\Delta E/kT)$ and $\Delta E\approx G$. The subscripts on the relaxation rates have the useful property that they represent the total change in the strong field quantum numbers of the electron and the nucleus. The factor $\alpha$ clearly depends on $H$ and $m$. The results which we calculate below are not very sensitive to $\alpha$, and it is possible to assign it a constant value for all of the transitions and all of the magnetic fields which we use. For our observation frequency of 13.6 kMc/sec and a temperature of 1.18°K, a suitable value is 0.58.

We require a brief notation for the transitions between the hyperfine levels and use $T_1(m)$ for the transition $(1/2,m)\leftrightarrow(-1/2,m)$; $T_0(m)$ for $(1/2,m-1)\leftrightarrow(-1/2,m)$; and $T_2(m)$ for $(1/2,m)\leftrightarrow(-1/2,m-1)$. The transition rates induced by a radio-frequency field are found from first-order time-dependent perturbation theory to be

$$\Phi_{m\to m}{}^\pm=[g\beta(H_{rf})_\perp]^2 2\pi\hbar^{-2}\phi(\omega)=\Phi_1(m), \tag{3a}$$

$$\Phi_{m\to m-1}{}^+=\Phi_{m-1\to m}{}^-$$
$$=[g\beta(H_{rf})_\parallel]^2 C^2(m)2\pi\hbar^{-2}\phi(\omega)=\Phi_0(m), \tag{3b}$$

$$\Phi_{m-1\to m}{}^+=\Phi_{m\to m-1}{}^-=\Phi_2(m)=0, \tag{3c}$$

where $\parallel$ and $\perp$ refer to the static field direction, $C^2(m)=[I(I+1)-m(m+1)]$; and $\phi(\omega)$ would usually be dismissed as the shape function for the line. If the line were truely homogeneous it would be; if the line is only effectively homogeneous, it is possible to formally define a $\phi(\omega)$, but its interpretation will be involved. When an observing frequency of 13.6 kMc/sec is used, $G\approx 13.6$ kMc/sec and $A\approx 285$ Mc/sec, and we find that $\Phi_0(m)\approx 10^{-3}\Phi_1(m)$ for the same amplitude of rf field in the proper direction to drive either transition. Also if we take into account the difference in $A$ and $B$ for this ion, $\Phi_2(m)$ is not strictly zero but has a maximum value for $H\perp z$ (where $z$ is the trigonal axis of the double nitrate) which is $\Phi_0(m)/2200$.

The presence of quadrupole coupling can increase the magnitude of $\Phi_2(m)$ for $H$ not parallel to $z$. It also contributes to $\Phi_0(m)$ and allows transitions for which $\Delta m=\pm 2$ and $\Delta M_S=\pm 1$. For some $m$, all of these rates are of the order of $P^2I^4/A^2$ times $\Phi_1(m)$, and may be effective for rather small static quadrupole interaction constants $P$. We ignore these processes if it is possible to do so.

## Microwave Probe Signals

The intensity of the paramagnetic resonance signal due to an allowed transition may always be expressed

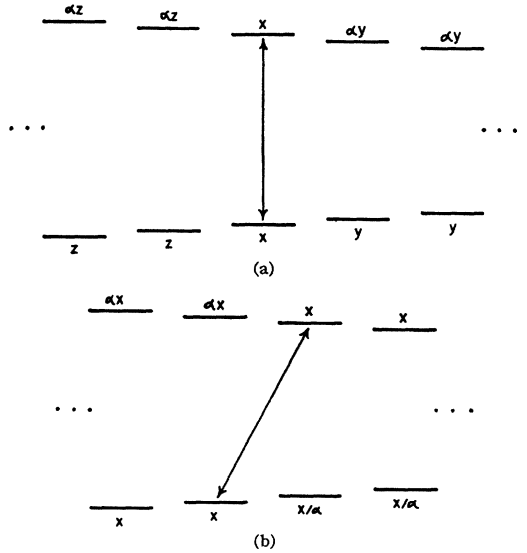


FIG. 2. (a) The populations of the hyperfine levels which result from the saturation of an allowed transition when the relaxation rates $W_0(m)$ and $W_2(m)$ are comparable. The values of $x$, $y$, and $z$ are calculated in Sec. II. (b) The populations produced by saturation of a forbidden transition when $W_1(m)$ is fast and $\Phi_2=0$.

in the form $\mathcal{S}_m=C(N_m^-{-}N_m^+)$ if the line is effectively homogeneous. The constant $C$ depends on the observing power used, the shape function $\phi(\omega)$, and the sensitivity of the spectrometer. The direct measurement of the intensity for a thermal equilibrium distribution of populations is adequate to establish that the constant $C$ is the same for all of the allowed transitions. The signal at thermal equilibrium is

$$\mathcal{S}_0=[Ca_m(1-\alpha)]/(1+\alpha), \tag{4}$$

where $a_m=N_m^+{+}N_m^-$ depends on the normalization used for the populations.

### Overhauser Effect

We assume that the allowed transition $T_1(m)$ is saturated with an rf field of the proper frequency and intensity. If we assume that the relaxation rates $W_1(m)$ are much faster than the slower of the two processes $W_0(m')$ or $W_2(m')$ for all $m'$, then except for the saturated transitions, all of the levels connected by $W_1(m')$ will have populations in the ratio determined by the Boltzmann factor characteristic of the lattice temperature. The populations will adjust to conform with this constraint and the saturation condition. The population distributions are shown in Fig. 2(a). It is apparent that the preceding conditions leave only three undetermined constants, which are denoted in the figure by $x$, $y$, and $z$. The rate equations corresponding to the steady-state yield two more constraints,

$$\begin{aligned}&(1+\alpha)dz/dt\\&=x[\alpha^{-1/2}W_0(m+1)+\alpha^{1/2}W_2(m+1)]\\&\quad-z[\alpha^{1/2}W_2(m+1)+\alpha^{1/2}W_0(m+1)]=0,\end{aligned} \tag{5a}$$

$$\begin{aligned}&(1+\alpha)dy/dt\\&=x[\alpha^{-1/2}W_2(m)+\alpha^{1/2}W_0(m)]\\&\quad-y[\alpha^{1/2}W_0(m)+\alpha^{1/2}W_2(m)]=0,\end{aligned} \tag{5b}$$

from which we find

$$\begin{aligned}z&=[x(1+\alpha R_m)]/[\alpha(1+R_m)],\\y&=[x(\alpha+R_{m+1})]/[\alpha(1+R_{m+1})],\end{aligned} \tag{6}$$

where $R_m=W_0(m)/W_2(m)$, and $x$ is to be determined by the normalization of the populations. When the signal for the allowed transition $T_1(m')$ is calculated, we find for $m'>m$,

$$\frac{\mathcal{S}^a(m',m)}{\mathcal{S}_0}=\frac{[(2I+1)(\alpha+R_{m+1})]}{\{(I-m)(\alpha+R_{m+1})+2\alpha[(R_m+1)/(1+\alpha)]+(I+m)(1+R_m\alpha)\}}, \tag{7a}$$

and for $m'<m$

$$\frac{\mathcal{S}^a(m',m)}{\mathcal{S}_0}=\frac{[(2I+1)(1+R_m\alpha)]}{\{(I+m)(1+R_m\alpha)+2\alpha[(R_m+1)/(1+\alpha)]+(I-m)(\alpha+R_{m+1})\}}. \tag{7b}$$

$\mathcal{S}^a(m',m)$ is the signal obtained from the allowed transition $T_1(m')$ when the allowed transition $T_1(m)$ is saturated. In the limit $R_m=0$ for all $m$, we find for $m'>m$

$$\frac{\mathcal{S}^a(m',m)}{\mathcal{S}_0}=\frac{(2I+1)\alpha}{\{(I-m)\alpha+[2\alpha/(1+\alpha)]+(I+m)\}}, \tag{8a}$$

and for $m'<m$,

$$\frac{\mathcal{S}^a(m',m)}{\mathcal{S}_0}=\frac{2I+1}{\{(I+m)+[2\alpha/(1+\alpha)]+(I-m)\alpha\}}; \tag{8b}$$

and, if $R_m=\infty$, Eqs. (8a) and (8b) are interchanged. If the sign of $A$ were negative rather than positive, Eqs. (7a) and (7b) would be interchanged.

It is apparent that if the sign of $A$ is known, the sign of $m$ for the saturated transition can be deduced from the position of the line on a magnetic field display at a constant observing frequency. The values of $R_m$ can be deduced if the signal ratios (7) are measured for all of the lines. If $R_m$ is essentially independent of $m$, the value can be deduced from a single signal measurement.

If the $T_1(m\pm1)$ transitions are saturated because of overlap effects, spin-spin processes, or because $W_1(m)$ is comparable to the smaller of the rates $W_0(m)$ and $W_2(m)$, all of the experimental data cannot be fitted with one set of $R_m$ values. The experimental data for $\mathcal{S}^a(m, m+1)$ will require a different set of $R_m$ than that for $\mathcal{S}^a(m, m-1)$. The theory developed in CUB predicts a small smooth variation of $R_m$.

### Saturation of Forbidden Transitions

We assume that an rf field at the proper frequency and with a component parallel to $H$ is applied with sufficient power to saturate the transition $T_0(m)$, and that $W_1(m)\gg W_2(m)$ so that a saturation of the adjacent allowed transition is not produced. The population distributions produced are shown in Fig. 2(b). The signals are

$$\frac{\mathcal{S}^f(m',m)}{\mathcal{S}_0}=\frac{(2I+1)\alpha}{(I-m+1)\alpha+(I+m)}, \quad m'\gtrless m, \tag{9a}$$

$$\frac{\mathcal{S}^f(m',m)}{\mathcal{S}_0}=\frac{2I+1}{(I-m+1)+(I+m)\alpha}, \quad m'<m, \tag{9b}$$

where $\mathcal{S}^f(m',m)$ is the signal obtained from observation of $T_1(m')$ when $T_0(m)$ is saturated. For $I\gg1$, these

effects are comparable to those for the Overhauser effects for $R_m=0$, Eqs. (8a) and (8b).

It is excessively difficult to calculate signals for the saturation of the forbidden transitions when $W_1(m) \approx W_2(m)$. The general effect is to produce saturation of the adjacent allowed transitions. If $W_1(m) \approx W_2(m) \approx W_0(m)$ saturation of an allowed or forbidden transition produces saturation of not only the adjacent transitions but smaller degrees of saturation for the allowed transitions farther removed from the saturated transition. In Appendix I, we give a treatment of the case where $W_1(m) \approx W_2(m)$ but $W_2(m) \gg W_0(m)$, because this is a case which we encounter in our experimental work. Our purpose at this point is only to develop equations suitable for the interpretation of relatively ideal situations.

## III. EXPERIMENTAL METHODS

### Nuclear Orientation

The double microwave resonance method used in the present experiments is similar to that used by Sorokin *et al.*[8] for their cross relaxation studies. The reader is referred to their paper for a drawing of the bimodal $TM_{110}$ cavity which is similar to ours except for the design frequency, which is about 13.6 kMc/sec in our case. The cavity has two irises; one couples the paramagnetic resonance spectrometer to one of the two orthogonal modes, which we refer to as the probe mode, and the other couples a VA-92 klystron (the pump) to the second mode, which we call the pump mode. The cavity is immersed in a helium bath which can be pumped to produce temperatures of $\approx 1.15$°K. A glass helium Dewar and the nitrogen Dewar outside of it hang in the 2.37-in. gap of a Varian electromagnet which has 12-in.-diam pole faces and a rotating yoke.

The paramagnetic resonance spectrometer used for the probe has been described briefly elsewhere.[9] The pump klystron can generate more than 100 mW of power and is coupled to the cavity through variable attenuators capable of producing 48 dB of attenuation. The microwave cavity modes are tuned by capacitive screws. A screw in the bottom plate tunes the probe mode and two others in the top plate tune the pump mode. One of the two top screws can be adjusted while the cavity is in the liquid-helium bath. If the bottom screw is adjusted so that the probe mode frequency $f_0$ is lower by 600 Mc/sec, the single top screw can be used to tune the pump mode frequency $f_p$ down until it is 600 Mc/sec lower than the probe mode. An attempt to produce much more separation with the single screw causes the coupling of the pump mode to become unusably small.

The probe measures the population difference of a selected $T_1(m)$ transition at a frequency $f_0$, while the pump mode is used to saturate a transition at the frequency $f_p=f_0+\Delta f$. To produce Overhauser effects, we use $\Delta f=\pm A, \pm 2A, \cdots$, where $A$ is the hyperfine interaction constant in frequency units. To saturate forbidden transitions, we require $\Delta f=\pm\frac{1}{2}A, \pm\frac{3}{2}A, \cdots$. Since $A\simeq 285$ Mc/sec in the present case, we can obtain a $\Delta f$ of $\pm 2A$. The field configurations of the two modes are orthogonal and it is possible to orient the static magnetic field relative to the cavity so that the rf magnetic field of the pump mode is parallel to the applied field whereas that for the observing mode is perpendicular to the field. This is ideal for the observation of nuclear orientation due to saturation of the forbidden transitions. Orientation due to saturation of the allowed transitions can be best observed with the static magnetic field so that it makes an angle of 45° with the rf magnetic field of either mode. To maintain these ideal conditions as one varies the direction of the static field relative to the crystal axes, the crystal must be rotated. We did not have room in the helium Dewar for such an arrangement and had to orient the crystal before insertion in the helium. Actually, in the observation of the Overhauser effects, usable amounts of power of the correct orientation were available in both modes for a full 90° rotation of the magnet. The variation of $(H_{rf})^2_\perp$ for either of the modes can be determined experimentally from the signal strength of the allowed transitions as the direction of the magnetic field is varied. The result depends on the crystal size and the amount of separation used for the modes but the extreme variation is usually between a factor of 10 and 100. For the observation of Overhauser effects this variation only requires that more power be used. In the saturation of the forbidden transitions the situation could be more critical. The forbidden matrix elements are smaller by a factor of 1000 than those for the allowed transitions in the present case, and the relaxation rates which we have determined are in some cases only smaller by a factor of 3. Unless we have nearly the optimum orientation of modes, the allowed transitions may be saturated because of a very slight overlap. We have treated this problem empirically by checking for saturation of the allowed transitions at the ends of the hyperfine structure with $\Delta f$ set either at $A/2$ or $-A/2$ so that it is on the wrong side to be on any transition of the hyperfine structure. (We refer to this later as the end-line test.) Such measurements have shown that except for the case where the static field is nearly 90° from the optimum, saturation by overlap is not important at powers which will saturate the forbidden transitions. Nevertheless, we have changed the crystal orientation so that no data need be taken when the rf fields and static fields were more than 45° from the optimum.

The resonance signals were detected with the usual magnetic field modulation and narrow band lock-in

[8] P. P. Sorokin, G. J. Lasher, and I. L. Gelles, Phys. Rev. **118**, 939 (1960).

[9] J. W. Culvahouse, W. Unruh, and R. C. Sapp, Phys. Rev. **121**, 1370 (1961).

detection and displayed on a strip chart recorder. The microwave bridge was balanced for dispersion so that the spectrometer signal (derivative of the dispersion with respect to magnetic field) was a maximum when the static magnetic field was at the center of the observed line. The magnetic field was modulated at a frequency of 37 cps for the most of the measurements, but detection circuits were available for 90 and 280 cps modulation, and were used to show that our results were independent of the modulation frequency in this range. The use of magnetic field modulation causes the overlap problem to be more severe because the frequency of the observed transitions during a part of the modulation cycle are nearer the frequency of the pump klystron. We found that our measurements were not affected if the peak-to-peak modulation amplitude was kept less than the rms linewidth (8 G compared with a 50-G separation of the hyperfine lines). Our measurements have indicated that the saturation of a transition does not depend on the frequency of the magnetic field modulation nor on the amplitude, if it is less than a linewidth. These results imply that the transitions are effectively homogeneous. We used the larger modulation amplitudes in most experiments because for some of the very low concentrations, all of the signal-to-noise ratio attainable was required.

For each experimental situation, the base line for zero signal was established, the equilibrium signal recorded, the pump klystron was tuned onto the cavity and the signal recorded as the pump power was increased in discrete steps.

## Crystals

The cobalt-doped $(La-Zn)\cdot(H_2O)$ crystals were grown at room temperature by evaporation of the aqueous solvent. Some very good crystals were obtained in this way; others were very cloudy, indicating the presence of occluded solution. The results of the paramagnetic resonance measurements did not depend on the optical quality of the crystal and some of the data presented in the next section were taken with very clear specimens, some with cloudy ones.

The concentration of the crystals grown is designated by a ratio of cobalt to zinc ions in the solution. We have checked the concentrations in the crystals by comparison of the cobalt paramagnetic resonance signals with those from a single crystal of $CuSO_4\cdot 5H_2O$. The concentrations in the crystals checked with those in the solutions within a factor of two for five crystals with concentrations between 0.5 and 0.005%.

The double nitrates grow in flat hexagonal plates, the plane of which is perpendicular to the trigonal or $z$ axis. These plates could be mounted directly on the bottom of the cavity for measurements made with $H\perp z$. For measurements with other orientations, flat plates were cut from a large hexagonal plate so that the plane of the plate contained the $z$ axis. In order to avoid a large preferential effect on the frequency of one of the orthogonal modes, the plates were all made square and oriented so that the dielectric loading was the same for the two modes. In defining the direction of the magnetic field relative to the crystal axis, we use the angle $\theta$ between the magnetic field and the symmetry axis and an angle $\varphi$ between the field direction and a plane which contains the symmetry axis and bisects one of the sides of the hexagonal plates. From the shape of the crystal, we cannot distinguish between $\varphi$ and $\varphi+60°$. The $\varphi$ defined here is not necessarily that used by CUB which is defined relative to the axes of the water octahedron. In all of the measurements reported here except in one set where $\varphi$ was varied, $\varphi$ is some multiple of 60°.

## Relaxation Times

The signal from the paramagnetic resonance spectrometer is proportional to the population differences between the two levels even in transient measurements if we assume that the line is effectively homogeneous and the coherence time $T_2$ is much shorter than the relaxation time. In this case it should make no difference whether dispersion or absorption effects are used to produce the signal because the two can be related by the Kronig-Kramers relations if the line shape does not change with time (as might occur with an inhomogeneous line).

No two levels of the hyperfine structure are isolated from all of the others, but we may asume as an approximation that the levels $(1/2,m)$ and $(-1/2, m)$ are connected by a relaxation process for which the rate constant is $W_1(m)$ and the other relaxation processes may be ignored. After saturation, the population difference will return to the thermal equilibrium distribution exponentially with the time constant

$$\tau_1(m)=[2W_1(m)\cosh(hf/2kT)]^{-1}=[2.07W_1(m)]^{-1},$$

in which $\cosh(hf/2kT)$ has been evaluated for $f=13.6$ kMc/sec and $T=1.18$°K. In all of our measurements there are always processes which tend to produce a more complicated recovery. In Appendix II, we describe an approximate method for the correction of observed relaxation times $\tau_1(m)$ for small values of $W_2(m)$ and $W_0(m)$. This correction is made assuming that the saturation of the allowed transition exists for such a short time that no appreciable nuclear orientation has developed by the Overhauser process. The uncorrected values are referred to as "apparent" relaxation times.

The "apparent" values of $\tau_1(m)$ were measured by this recovery from a short saturation pulse using the cavity described above. $\Delta f$ was set at about 30 Mc/sec which is to be compared with the full width at half-maximum for the transitions of about 70 Mc/sec. The repeller voltage of the pump klystron was stepped from a value where the klystron did not oscillate to a value for which it oscillated at the frequency of the pump

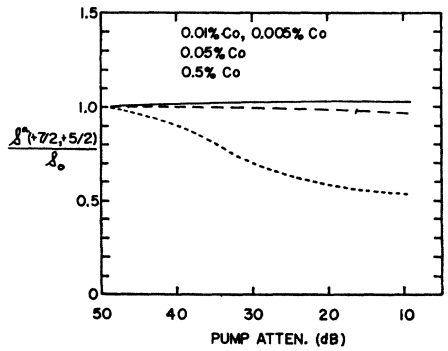


FIG. 3. The signal from the transition $T_1(+7/2)$ as increasing power is applied to $T_1(+5/2)$ for four concentrations of cobalt and $H \perp z$. The attenuation here and in subsequent figures is the setting of the variable attenuators in front of the pump klystron. The lowest curve corresponds to the highest concentration. The curves for the two lowest concentrations cannot be distinguished.

mode for 15 msec and then was stepped out of oscillation for 500 msec. The reflector voltage modulation was taken from a fast bistable multivibrator which was triggered by a series of negative pulses generated by an unsymmetrical multivibrator and pulse-shaping circuits. The rectified dc output of the superheterodyne detector was displayed on the $y$ axis of a Tektonix 545 scope with a type CA preamplifier. The $x$-axis sweep was normally triggered by the pulse which turned the saturating power off of the cavity. The display of the signal recovery from saturation was photographed and later used to make semilogarithmic plots.

It was possible to switch the pump klystron off of the pump mode in less than $10^{-6}$ sec. The response time of the detection circuits was limited by the i.f. filter and was about $10^{-5}$ sec. It was not possible to turn the klystron onto the pump mode in less than 1 msec because the frequency of the klystron drifts some after the voltage pulse is applied, and must be allowed to coast into the cavity mode with its own time constant.

The pump power is well enough isolated from the spectrometer by the cavity that it is possible to observe the line while it is saturated. Since we were unable to turn the pump power on to a steady value in a really short time, we could only verify that the saturation spread over essentially all of the line in 5 msec.

## IV. EXPERIMENTAL RESULTS

The data reported here were taken at 1.18°K and with the spectrometer operating at a frequency within a few percent of 13.6 kMc/sec unless explicitly stated otherwise. The data have been taken over a period of 18 months in about 50 separate low-temperature runs. For crystals of adequately low concentration, the results are highly reproducible even when taken with crystals of varying optical quality.

As the data are discussed, reasons for the deviations from the ideal theory are stated without qualification. The validity of our explanations is examined in Sec. V.

### Concentration Effects

Double microwave frequency measurements of the effects produced by saturation of forbidden transitions and those produced by saturation of allowed transitions have been made for cobalt concentrations of 0.5, 0.05, 0.01, and 0.005%. Crystals with concentrations of 0.5% always showed a strong saturation of the allowed transitions adjacent to the transition for which the pump frequency was equal to the resonant frequency of the transition. This is true whether the transition which is supposed to be saturated is an allowed or forbidden one. It was demonstrated that this is not an overlap problem by means of the end-line

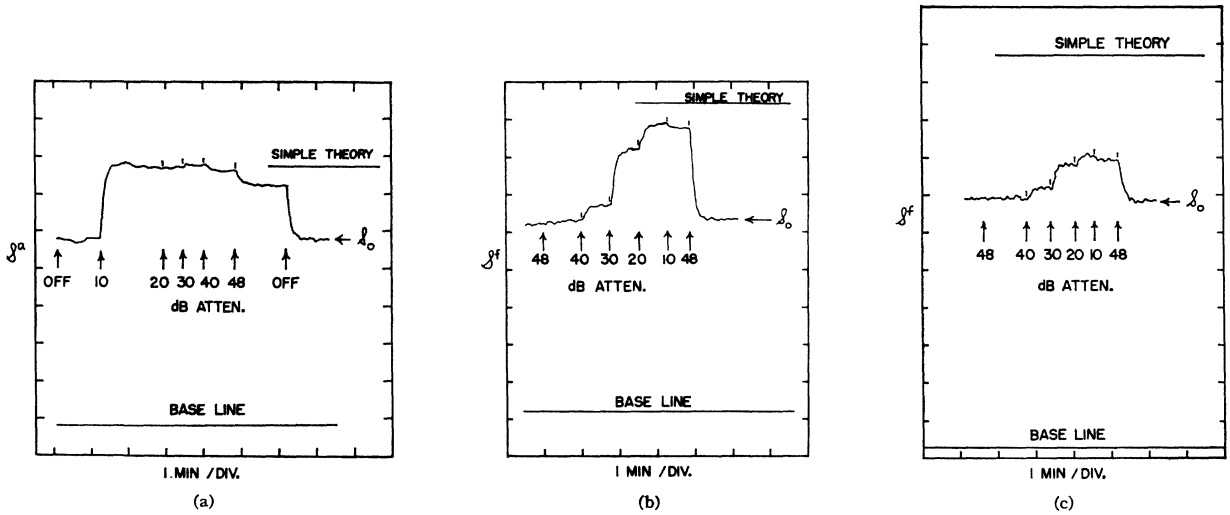


FIG. 4. (a) The signal from $T_1(-5/2)$ as decreasing power is applied to $T_1(-3/2)$ for $H \| z$. (b) The signal from $T_1(-7/2)$ as increasing power is applied to $T_0(-5/2)$ for $H \perp z$. (c) The same as (b) but for $H \| z$.

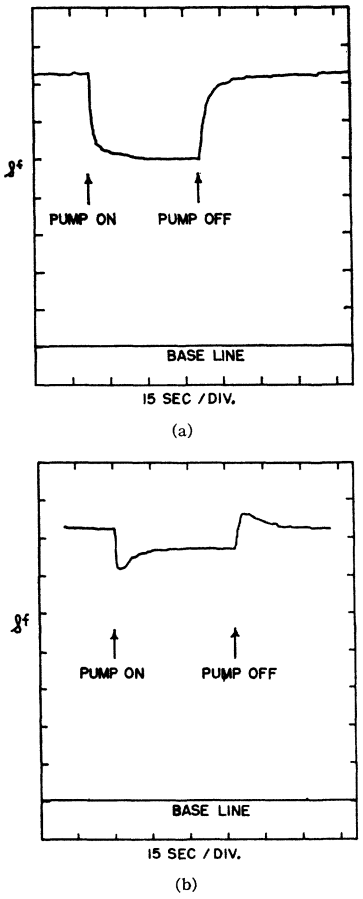


FIG. 5. (a) Transient behavior of the signal from $T_1(+7/2)$ after saturating power is applied to $T_0(+7/2)$ and then removed, for $H\perp z$. (b) Transient behavior of the signal from $T_1(-5/2)$ when saturating power is applied to $T_0(-3/2)$ and then removed, for $H\perp z$.

test described in Sec. III. We have interpreted this effect as evidence of cross relaxation between hyperfine lines. In Fig. 3 the signal from $T_1(+7/2)$ is shown as a function of pump power applied to $T_1(+5/2)$ for several concentrations of cobalt. It is apparent that the saturating effects are no longer present for concentrations of 0.01 and 0.005%. The small increases for low concentrations is an Overhauser effect. That it is unaffected by cross relaxation is established in part by the lack of change between 0.01 and 0.005%, and in part by measurements at other angles which produce full Overhauser effects for the low concentrations.

## Nuclear Orientation Data

Figure 4(a) is the signal obtained from the transition $T_1(-5/2)$ for $H\|z$ when the transition $T_1(-3/2)$ is driven with decreasing amounts of pump power. The effect produced with 10 dB attenuation of the pump power agrees with the prediction of the simple theory and there is no change in the effect for a reduction of the power by two orders of magnitude.

In Fig. 4(b), a similar chart is given for the signal from $T_1(-7/2)$ when $T_0(-5/2)$ is saturated for $H\perp z$. In this case the power dependence is much different and after an initial increase to a value very near that predicted by the simple theory, the signal begins to decrease. This slight decrease could be due to overlap because we do have some rf field perpendicular to $H$ and the amount of decrease is within the limits of accuracy of the end-line test.

The signal for the $T_1(-7/2)$ transition while $T_0(-5/2)$ is saturated is shown for $H\|z$ in Fig. 4(c). In this case the maximum value is considerably less than the theoretical value. Again, the decrease at the high power is within the accuracy of the end-line test and, if real, may be due to overlap.

## Transient Nuclear Orientation

As is apparent from Fig. 4, the complete redistribution of population requires a time that can be measured on the chart recorder. The transient effects are displayed in Fig. 5(a), which shows the signal from line $T_1(-7/2)$ for $H\perp z$ after saturating power has been applied suddenly to $T_0(-5/2)$, and then, after a delay, removed suddenly. The decay appears to be closely exponential, but it must represent the effect of all of the relaxation processes and be separable into several exponential decays. A more striking demonstration is given in Fig. 5(b) in which the transition $T_1(-5/2)$ is observed while the transition $T_0(-5/2)$ is saturated suddenly. The initial effect occurs so rapidly that it appears instantaneous on the chart record and may be attributed to the adjustment of the population of the levels $(\pm 1/2, -5/2)$ and $(\pm 1/2, -7/2)$ which occurs within a few multiples of $1/W_1(-5/2)+1/W_1(-7/2)$. The later development corresponds to the complete redistribution of populations. The initial effect, if it were to develop fully, would be

$$S^f(-5/2, -5/2)/S_0 = 2(1+\alpha)/(2+\alpha+\alpha^{-1}) = 0.76,$$

whereas the final effect predicted by Eq. (9) would be 0.92. This agrees rather well with the measurements.

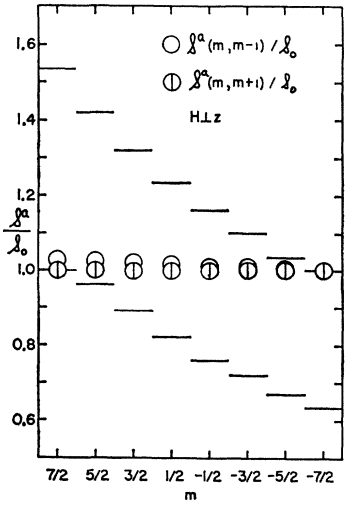


FIG. 6. The measured signals from $T_1(m)$ when $T_1(m+1)$ and $T_1(m-1)$ are saturated, for $H\perp z$. The histograms are drawn according to the theory of Sec. II, with $R_m=\infty$.

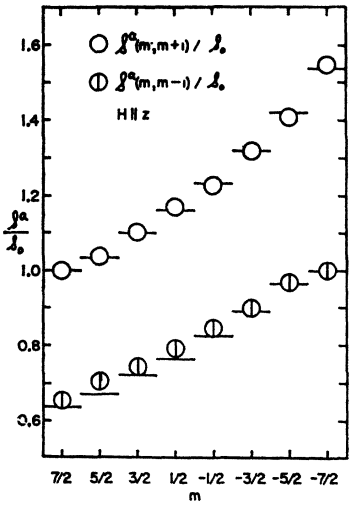


FIG. 7. The measured signals from $T_1(m)$ when $T_1(m+1)$ and $T_1(m-1)$ are saturated, for $H\|z$. The histograms are drawn according to the theory of Sec. II, with $R_m=0$.

TABLE I. Transition rates for $Co^{2+}$ in $La_2Zn_3(NO_3)_{12}\cdot 24H_2O$ in $sec^{-1}$.

| $m$ | Exp. $W_1(m)$ | Corr. $W_1(m)$ | Theoretical $W_1(m)$ | $W_0(m)$ | $W_2(m)$ |
|---|---|---|---|---|---|
| | | | (a) $H\perp z$ | | |
| 7/2 | 53.7 | ··· | 50.5 | 0.80 | 0.40 |
| 5/2 | 80.5 | ··· | 46.0 | 1.34 | 0.68 |
| 3/2 | 43.1 | ··· | 42.4 | 1.58 | 0.85 |
| 1/2 | 37.2 | ··· | 39.6 | 1.60 | 0.91 |
| −1/2 | 33.3 | ··· | 34.7 | 1.42 | 0.85 |
| −3/2 | 28.4 | ··· | 32.2 | 1.09 | 0.68 |
| −5/2 | 28.0 | ··· | 28.4 | 0.60 | 0.40 |
| −7/2 | 22.0 | ··· | 25.5 | ··· | ··· |
| | | | (b) $H\|z$ | | |
| 7/2 | 11.2 | 10.1 | 11.4 | 0 | 2.09 |
| 5/2 | 11.2 | 8.2 | 10.4 | 0 | 3.60 |
| 3/2 | 10.7 | 6.5 | 9.6 | 0 | 4.50 |
| 1/2 | 9.7 | 5.2 | 8.95 | 0 | 4.80 |
| −1/2 | 9.1 | 4.6 | 7.85 | 0 | 4.50 |
| −3/2 | 7.5 | 4.6 | 7.05 | 0 | 3.60 |
| −5/2 | 6.5 | 3.9 | 6.43 | 0 | 2.09 |
| −7/2 | 5.3 | 4.5 | 5.76 | ··· | ··· |

## General Survey of the Overhauser Effects

For $H\perp z$, the Overhauser effects are all very small. These are plotted in Fig. 6 for the observation of $T_1(m)$ when $T_1(m-1)$ is saturated ($\Delta f=-A$) and for $T_1(m)$ when $T_1(m+1)$ is saturated ($\Delta f=+A$). The theoretical results for $R_m=\infty$ are indicated in histogram form for reference. It is apparent that $R_m\approx 1$.

The Overhauser effects for $H\|z$ are plotted in Fig. 7 for the same set of experimental situations. The theory for $R_m=0$, $W_2(m)\gg W_0(m)$, is given by the histogram and the agreement is very good.

The Overhauser effect changes monotonically as the angle $\theta$ between the magnetic field and the $z$ axis is varied from $\theta=0°$ to $\theta=90°$. The results for $T_1(-7/2)$ when $T_1(-5/2)$ is saturated and for $T_1(7/2)$ when $T_1(+5/2)$ is saturated are given in Fig. 8, as a function of $\theta$. The curves are according to the theory discussed in the next section.

## General Survey of the Jeffries Effects

Figure 9 shows the signal obtained from $T_1(m)$ when $T_0(m)$ is saturated ($\Delta f=-A/2$) and from $T_1(m)$ when $T_0(m+1)$ is saturated ($\Delta f=+A/2$) for $H\|z$. The experimental results are in extreme disagreement with the simple theory of Sec. II. The explanation for this disagreement is that $W_2(m)$ is not much smaller than $W_1(m)$. The dotted histograms given in Fig. 9 represent the values calculated from the theory of Appendix I, in which the theoretical values for the ratio $W_1(m)/W_2(m)$ derived in the next section have been used.

In Fig. 10, the results for the signal from $T_1(m)$ when $T_0(m-1)$ is saturated ($\Delta f=-3A/2$) and when $T_0(m+2)$ is saturated ($\Delta f=+3A/2$) are compared with the simple theory. The agreement with the simple theory is also in accord with the theory of Appendix I.

In Fig. 11, similar results for $\Delta f=\pm A/2$ are plotted for $H\perp z$. The agreement with the simple theory is much better. This is because the ratio of $W_1(m)/W_2(m)$ is much larger for this angle. The values obtained for $\Delta f=\pm 3A/2$ are in excellent agreement with the simple theory.

## Allowed Relaxation Rates

Pulsed microwave measurements of the apparent relaxation times $\tau_1(m)$ have been made for all eight of the allowed transitions as a function of the angle between the direction of $H$ and the $z$ axis. The results for $H\perp z$ and $H\|z$ for all $m$ values are tabulated in Table I.

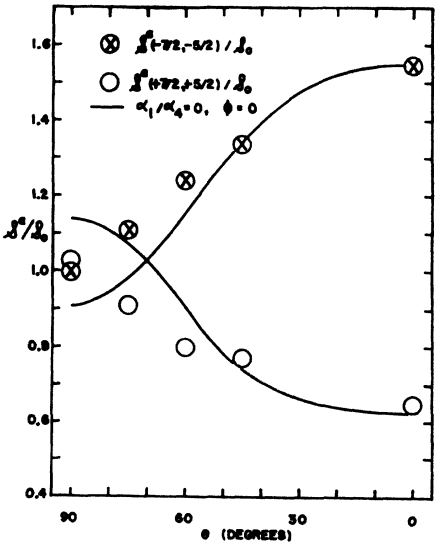


FIG. 8. The measured signals from $T_1(-7/2)$ when $T_1(-5/2)$ is saturated, and from $T_1(+7/2)$ when $T_1(+5/2)$ is saturated, as a function of the angle $\theta$ between $H$ and $z$. The curves are drawn according to the theory of Sec. V.

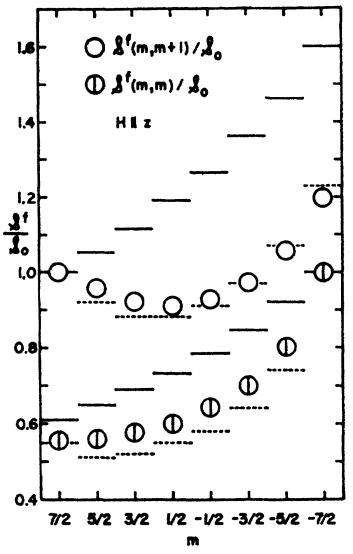


FIG. 9. The measured signals from $T_1(m)$ when $T_0(m)$ and $T_0(m+1)$ are saturated, for $H\|z$. The solid histograms are drawn according to the theory of Sec. II, and the dashed histograms are calculated in Sec. V.

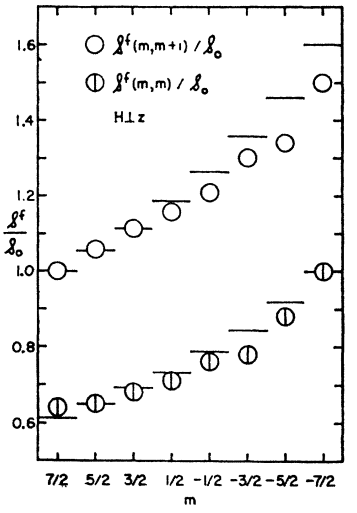


FIG. 11. The measured signals from $T_1(m)$ when $T_0(m)$ and $T_0(m+1)$ are saturated, for $H\perp z$. The histograms are drawn according to the theory of Sec. II.

The allowed relaxation times are all faster for $H\perp z$. The Overhauser effects in that case imply $W_2(m)\approx W_0(m)$, and the Jeffries effects imply $W_2(m)\ll W_1(m)$. We can therefore conclude that the correction of the observed relaxation times is very slight for $H\perp z$.

For $H\|z$, we know from the Jeffries and Overhauser effects that $W_1(m)$ is not vastly larger than $W_2(m)$ so that some correction of the relaxation times must be made. This correction is considered in Sec. V, but we note that it is fairly small for the $m=+7/2$ transition which is the fastest. We have, therefore, given a plot of $\tau_1(+7/2)$ as a function of $\theta$ in Fig. 12.

We have measured the allowed relaxation rates as the direction of the magnetic field is varied in the plane perpendicular with the symmetry axis ($\theta=90°$). No variation was observed outside the experimental error of about 10%. Since the theory predicts a maximum variation with the azimuthal angle when $\theta$ is near 60°, we made the following measurements: The flat hexagonal plate was set on a polyfoam ramp which caused the symmetry axis to tilt 60° from the horizontal plane and to lie in a vertical plane which bisected one of the interior angles of the hexagonal plate. The direction of the magnetic field was then rotated in the horizontial plane. As a result of varying $\phi$, there is some variation of $\theta$, $\cos\theta=0.5\times\cos(\Delta\phi)$, where $\Delta\phi$ is the angle that the field lies out of the vertical plane containing the symmetry axis. The results for this measurement are presented in Fig. 12(b). The solid curve is calculated with the theory of CUB, and the dashed curve is the variation expected from the changes in $\theta$ alone. The relaxation rates are the same at any multiple of 60° which explains why we were able to get reproducible results in our earlier measurements by orienting the crystals relative to their faces.

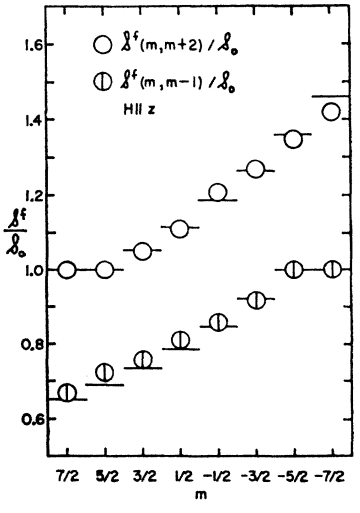


FIG. 10. The measured signals from $T_1(m)$ when $T_0(m-1)$ and $T_0(m+2)$ are saturated, for $H\|z$. The histograms are drawn according to the theory of Sec. II.

## Temperature Dependence of the Allowed Relaxation Rates

The relaxation times for all allowed transitions have been measured for $\theta$ between 0° and 90° in the temperature range from 1.18 to 4.2°K. The results are plotted in Fig. 13 for the magnetic field perpendicular and parallel to the symmetry axis for $m$ of $\pm 7/2$. Up to a temperature of 2°K, the relaxation times vary nearly as $\tanh(hf/2kT)\approx hf/2kT$ as would be expected for a direct process. Above that point, the variation is more rapid and all of the allowed relaxation rates become the same. From a log-log plot of $1/\tau$ vs $T$ using the points plotted in Fig. 13 and some other data not presented there, one finds that the allowed rates may be written: $1/\tau=aT+bT^9$, where $a$ is different for each transition and direction of applied field and can be calculated from the rates at 1.18°K, and $b=1.9\times10^{-3}$ $\text{sec}^{-1}$ $\text{deg}^{-9}$ for all field directions and all transitions. This temperature variation is in agreement with that

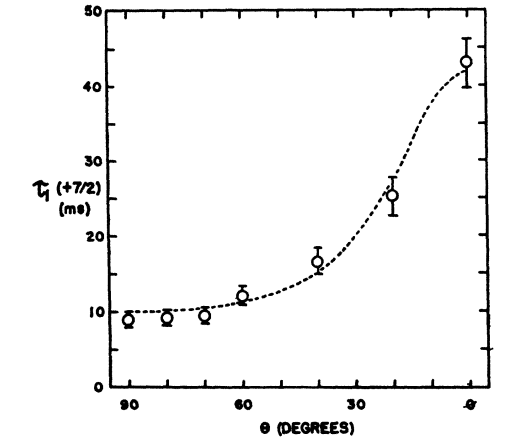


(a)

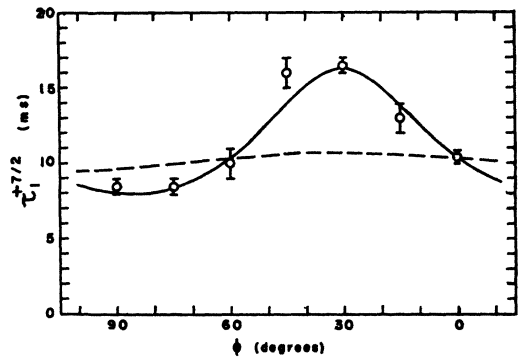


(b)

FIG. 12. (a) The apparent relaxation time for $T_1(+7/2)$ as a function of the angle $\theta$ between $H$ and $z$, for $\phi=0$. The curve is the theoretical prediction derived in Sec. V. (b) The variation of the apparent relaxation time as the direction of the field is varied in the horizontal plane with the symmetry axis tilted by 30° from the vertical. $\phi=30°$ defines the vertical plane in which the symmetry axis lies. The zero value of $\phi$ corresponds to the bisector of one of the hexagonal faces of the crystal. The dashed line shows the change in the relaxation times because of the changes in $\theta$. The solid curve is according to the theory in Sec. V.

for a direct process and a Raman process for a Kramers doublet.[10]

## V. COMPARISON WITH THEORY

### Evaluation of Parameters

The temperature variation of the relaxation rates suggest that we are dealing with direct relaxation processes between 1.18 and 2°K. We, therefore, use the theory of the preceding paper in an attempt to fit the data.

We begin by considering the ratio of the allowed relaxation rates for $H\perp z$ and $H\|z$. This ratio and Eq. (56) of CUB yields the following relation between the constants $\alpha$:

$$(4\alpha_4+2\alpha_3+\alpha_2)=15.6(\alpha_4-\alpha_3+\alpha_2). \quad (10)$$

[10] R. Orbach, Proc. Phys. Soc. (London) A77, 821 (1961).

From the change in the allowed relaxation rates between $\phi=0°$ and 30° shown in Fig. 12(a) and Eq. (56), we find

$$(2\alpha_4-\alpha_3-\alpha_2)=\pm 3.36(\alpha_4-\alpha_3+\alpha_2). \quad (11)$$

The two choices of sign in (11) depend upon the two possible choices of $\phi$ mentioned in Sec. III.

The results for the Overhauser effect for $H\|z$ imply that $R_m\leq 0.02$. This number combined with Eqs. (55) of CUB gives the result: $(1+f(m))^2\alpha_1\leq 0.16(4\alpha_4+2\alpha_3+\alpha_2)$. We assume that the constant $\Gamma$ defined by CUB has the value 3.25 calculated theoretically and that $A_0/g\beta H=1/48$. With these numbers we obtain

$$\alpha_1\leq 0.06(4\alpha_4+2\alpha_3+\alpha_2). \quad (12)$$

Solving these equations with the plus sign in Eq. (11) yields the results: $\alpha_3/\alpha_4=0.81$, $\alpha_2/\alpha_4=0.12$, and $\alpha_1/\alpha_4\leq 0.34$. Consistency of the results require that $\alpha_3\leq 2(\alpha_2\alpha_4)^{1/2}$; thus our value of $\alpha_2/\alpha_4$ requires $\alpha_3/\alpha_4\leq 0.70$.

Solution of the equations with a minus sign in (11) yields: $\alpha_3/\alpha_4=2.30$, $\alpha_2/\alpha_4=1.98$, and $\alpha_1/\alpha_4<0.63$. The consistency requirement is $\alpha_3/\alpha_4\leq 2.80$.

These two sets of constants give precisely the same predictions for all of the relaxation rates when used with the proper choice of the angle $\phi$.

The product of the constant $\alpha_4$ and the factor $\mathcal{W}$ is

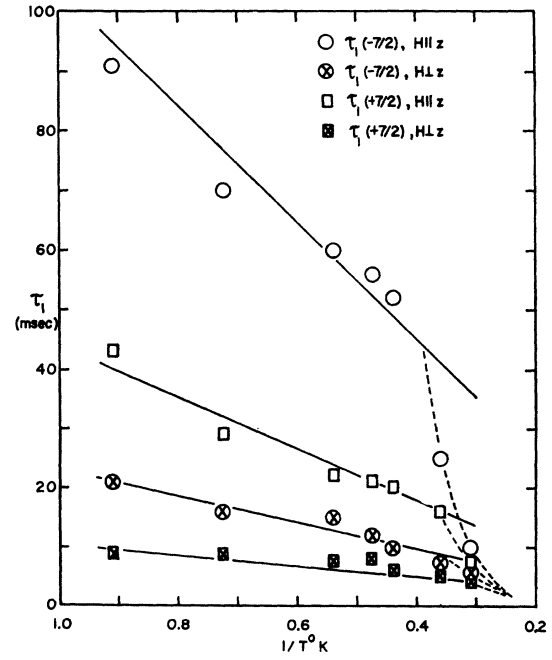


FIG. 13. The temperature dependence of the apparent relaxation rates for the transitions $T_1(+7/2)$ and $T_1(-7/2)$, for $H\perp z$ and $H\|z$. The solid lines are drawn for a $1/T$ variation. The dashed lines show the behavior of the experimental data at higher temperatures where it is not possible to make distinct plots for the separate data points. For clarity, the error bars have been omitted; the errors are ±10%.

chosen so that the relaxation rate for the allowed transition for $m=+7/2$ and $H\perp z$ is 51 sec$^{-1}$.

### Angular Variation of the Allowed Rates

Substituting the constants into Eq. (56), and allowing for the variation of the magnetic field with the transition that is observed, we obtain an expression for the allowed relaxation rates for any direction of the applied magnetic field:

$$W_1(m)=3.22[1+0.048m -7.5\times10^{-4}(15.75-m^2)/(1-0.02m)]^2 \times\{10.24(\sin^2\theta)(1+\cos^2\theta)+1.31[(\cos^2\theta-\sin^2\theta)^2 +\cos^2\theta]-9.75\sin^3\theta\cos\theta\sin(3\phi)\}, \quad (13)$$

in which we have taken $\alpha_1=0$. This expression is plotted in Fig. 12(a) as a function of $\theta$ with $\phi$ taken as zero. The agreement with experiment is excellent. At $\theta=45°$, the allowed relaxation rates are most sensitive to the value of $\alpha_1$. If $\alpha_1$ is given the largest value allowed by the Overhauser results, the relaxation rates at 45° are changed by less than 5%. Therefore the limits on $\alpha_1$ given by the Overhauser effect are the most stringent.

Equation (13) has been used to predict the experimental results when both $\theta$ and $\phi$ vary as in the experimental data plotted in Fig. 12(b). The agreement is adequate in view of the possibility of errors in the orientation of the crystal for that experiment.

### Angular Variation of the Overhauser Effect

Using Eqs. (55) of CUB, and assuming that $\alpha_1=0$, we find for the relaxation rates between levels for which the nuclear spin is different

$$W_0(m)=3.74\times10^{-3}[1.62+0.021(2m-1)(1+0.02m)]^2 \times C^2(m-1)(10.24\sin^4\theta+5.24\cos^2\theta\sin^2\theta -9.75\sin^3\theta\cos\theta\sin3\phi), \quad (14)$$

and

$$W_2(m)=3.74\times10^{-3}C^2(m-1)[10.24(\cos^4\theta+6\cos^2\theta+1) +5.24(\sin^2\theta)(1+\cos^2\theta) -9.75\sin^3\theta\cos\theta\sin3\phi]. \quad (15)$$

From these equations, the ratio $R_m$ can be calculated as a function of $\theta$. We have used the values of $R_m$ obtained in this way to predict the signal ratios produced in an Overhauser experiment. The theoretical predictions are compared with experiment in Fig. 8. The agreement at $\theta=0°$ was put into the parameters by chosing $\alpha_1=0$. Beyond 45° from the symmetry axis there is a definite disagreement of theory and experiment. We believe that this deviation can be attributed to a small static quadrupole effect. The static quadrupole effects does not affect the Overhauser effect near the symmetry axis but at large $\theta$ a very small value for $P$ can have large effects. For example, a static quadrupole splitting would allow an rf matrix element for the

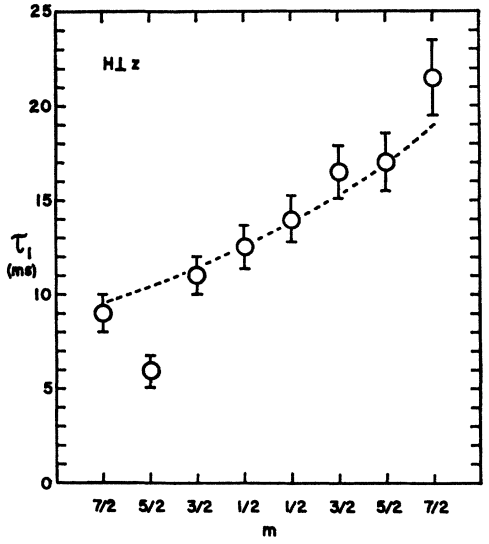


FIG. 14. The relaxation rates for $T_1(m)$ at $H\perp z$. The curve is predicted by the calculations of Sec. V.

transitions $(1/2,m)\leftrightarrow(-1/2,m-2)$ and $(-1/2,m)\leftrightarrow(1/2,m-2)$ which are at the same frequency as $T_1(m-1)$. At $\theta=90°$, $P/A\approx10^{-2}$ would yield a transition rate for this process of about $\Phi_1/100$.

### Dependence of the Allowed Rates on $m$

Equations (13), (14), and (15) give predictions for all of the relaxation times. For $H\perp z$, the equations predict that $W_2(m)\approx W_0(m)\leq(1/20)W_1(m)$. The measured values of $\tau_1(m)=[2.07W_1(m)]^{-1}$ should, therefore, agree with the theory which predicts a variation as $[F(m)]^{-2}(1-0.02m)^2$. The comparison is made in Fig. 14. The agreement is within experimental error except for $m=+5/2$. This deviation was checked many times and is very real. The key to an explanation seems to be that for $H\perp z$, the forbidden transition (the $\Delta M_S=\pm2$ transition) of divalent nickel in the $X$ site precisely overlaps this cobalt line. The allowed lines of divalent nickel could not be observed, but this is possible because the linewidth of the allowed transitions is very broad. In (La—Mg)·($H_2O$) the overlap occurs only for a limited range of observing frequencies near 13.6 kMc/sec. For $H\|z$, the relative position of the nickel line and those of cobalt shift by about 2/3 of the spacing of the cobalt hyperfine lines.

The observations of $\tau_1(m)$ for $H\|z$ are severely affected by $W_2(m)$. In Appendix II, we derive approximate corrections for the effect of $W_2(m)$. We have used those results and the theoretical values for $W_2(m)$ to obtain a corrected value for $W_1(m)$. The apparent and corrected values for $W_1(m)$ are tabulated in Table I as well as the theoretical values for all relaxation rates for $H\perp z$ and $H\|z$. Unfortunately, the corrections to $W_1(m)$ for $H\|z$ are so large in most cases that the correction method is clearly invalid and overcorrects.

The corrected values for the two end transitions should be reasonably valid. Since the correction for the $m=+7/2$ transition is not negligible, we should recalculate the constants $\alpha_i$ so to fit that result. We have not done so because the only significant effect would be to change the constants $\alpha_i$ slightly. The corrected relaxation rates for $m=\pm 7/2$ are very nearly in the correct ratio required by the $m$ variation in Eq. (13).

### Jeffries Effects

We have noted already that the theory predicts $W_2(m)\approx W_0(m)\leq(1/20)W_1(m)$ for $H\perp z$ so that the simple theory agrees fairly well with experiment. Also it predicts deviations from the simple theory for $H\|z$. We have made a quantitative comparison by using the results from Appendix I to calculate the signals produced when $W_2(m)$ and $W_0(m)$ have the values predicted by the theory. These values are tabulated in Table I. The results for the Jeffries effect are given in Fig. 9. The agreement is not perfect and is off by nearly 10% for some of the signals, but the large improvement over the ideal theory is impressive. The theoretical results for the signals from the transitions further removed from the transition which is being saturated are essentially the same as the results of the ideal theory, and have not been shown in Fig. 10. These results substantiate the essential accuracy of the theoretical relaxation rates.

### Transient Nuclear Orientation

As a further test of the validity of the theoretical predictions for the relaxation rates, we have set up a circuit analog which simulates the behavior of the 16 level populations.[10] The relaxation times in the circuit were set according to the theoretical values of the relaxation rates tabulated in Table I, and the initial level populations were set to the theoretical values for a steady state Overhauser or Jeffries effect. The signal changes after the steady-state saturation was removed were obtained from the analog and compared with experimental data such as those in Figs. 5(a) and 5(b). The shape and time scales agreed within 10% for all situations which were simulated.

## VI. CONCLUSIONS

Only four experimental measurements have been used to evaluate the constants $\alpha_i$ in the theory: (a) The relaxation time for one of the allowed transitions with $H\perp z$. (b) The relaxation time for the same allowed transition with $H\|z$. (c) The relative values of two allowed relaxation rates at two values of $\phi$. (d) The Overhauser effect for $H\|z$. The agreement of the theoretical results with the remainder of the experimental results constitute a strong verification of the validity of the theory presented in the preceding paper.

The most serious discrepancy between theory and experiment is for the Overhauser effect with $H\perp z$. The deviation of the experimental results from theoretical predictions shown in Fig. 6 would correspond to an error factor of about 1.5 in the ratio $R_m$ for $\theta=90°$. It is possible that the very small Overhauser effect can be the result of the saturation of transitions such as $(-1/2, m-2)\leftrightarrow(1/2,m)$ because of a very small static quadrupole interaction.

The order of magnitude of the constants $\alpha_i$ that are required are not inconsistent with those that can be calculated from a Debye phonon spectrum and a dipole or charge model for the crystal field. Our most significant result in this aspect of the work is that $\alpha_3$ which would be zero for a crystal of cubic or higher symmetry has nearly the extreme value for trigonal symmetry. In simple terms, this result implies that the water molecules have much different amplitudes of vibration along the symmetry axis than perpendicular to it. Such a result is not unexpected. The change in the zero field splitting of nickel ions with temperature[11] implies such anisotropic properties.

The demonstration of an Overhauser effect corresponding to $R_m=0$, rather than $R_m=\infty$ as is usually assumed, and the angular dependence of the effect highlight the danger in assuming that hyperfine relaxation effects (even for an isotropic static hyperfine interaction) obey a selection rule of $\Delta(m_I+M_S)=0$.

We have verified the prediction made by CUB that the hyperfine relaxation effects may be very important even when the applied field is so strong that the second-order hyperfine effects are almost undetectable in the paramagnetic resonance spectrum. Because of the particular values of the constants $\alpha_i$, the relaxation $W_2(m)$ is virtually as fast as that for the allowed transition for $H\|z$. If the applied field were appreciably smaller, the relaxation rates would be entirely dominated by the dynamic hyperfine interaction.

It does not seem possible for us to contribute anything to the understanding of the experiment of Abraham *et al.*[12] on the orientation of $Co^{60}$ in $(La-Mg)\cdot(D_2O)$. Our result for the Overhauser effect in $(La-Zn)\cdot(H_2O)$ implies that the gamma-ray anisotropy produced by the Overhauser and Jeffries effects for $H\|z$ will have the same sign and not the opposite as was assumed in reference 12. Even with this added information, a complete interpretation is not possible. At a $Co^{59}$ concentration of 0.6% as used in the work of Abraham, we have found that the saturation of a single transition of the $Co^{59}$ hyperfine structure disturbs the populations of all of the levels of the $Co^{59}$; and these redistributions affect the $Co^{60}$ populations by spin-spin

[10] A computer similar to the one used by us has been described by F. M. Pipkin, G. E. Bradley, and R. E. Simpson, Nucl. Phys. 27, 353 (1961).

[11] J. W. Culvahouse, J. Chem. Phys. 36, 2720 (1962).

[12] M. Abraham, C. D. Jeffries, and R. W. Kedzie, Phys. Rev. 117, 1070 (1960).

interactions. We agree with the conclusion of reference 12 that there is no Overhauser effect for $H \perp z$.

## APPENDIX I: JEFFRIES EFFECT FOR SLOW ALLOWED RELAXATION RATES

Figure 15 shows the level populations produced by the saturation of a forbidden transition when $W_2(m) \approx W_1(m) \gg W_0(m)$. The values of $x$, $y$, and $z$ are to be determined from the rate equations for the $W_1(m)$

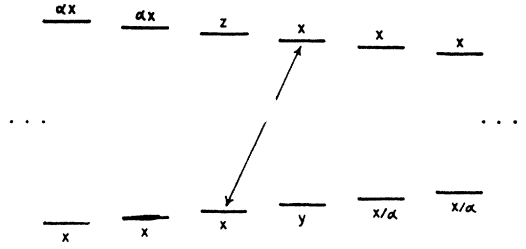


FIG. 15. The energy levels for the hyperfine structure ($A>0$) and the populations produced by saturation of $T_0(m)$ when $W_2(m) \approx W_1(m)$. The values of $x$, $y$, and $z$ are calculated in Appendix I.

and $W_2(m)$ relaxation processes and the normalization condition. The rate equations are

$$dz/dt = \alpha^{1/2}[xW_1(m)+yW_2(m)] - \alpha^{-1/2}[W_1(m)+W_2(m)]z = 0,$$

and

$$dy/dt = \alpha^{-1/2}[xW_1(m-1)+zW_2(m)] - \alpha^{1/2}[W_1(m-1)+W_2(m)]y = 0,$$

from which we find

$$z/x = [\alpha(1+P_m')+P_m]/[1+P_m+P_m'],$$
$$y/x = [\alpha^{-1}(1+P_m)+P_m']/[1+P_m+P_m'],$$

where $P_m' = W_2(m)/W_1(m-1)$ and $P_m = W_2(m)/W_1(m)$. The normalization condition yields for $x$ the value

$$x = (2I+1)/\{(I-m)(1+\alpha) + (I+m-1)(1+\alpha^{-1}) + [(z+y)/x]+2\}.$$

The signals are then to be calculated from the population differences of the allowed transitions.

## APPENDIX II: CORRECTION OF ALLOWED RELAXATION RATES

The rate equation for the population difference $N_m^+ - N_m^-$ is

$$\begin{aligned} d(N_m^- - N_m^+)/dt = &-2W_1(m)[-\alpha^{1/2}N_m^- - \alpha^{-1/2}N_m^+] \\ &- W_0(m)[\alpha^{1/2}N_m^- - \alpha^{-1/2}N_{m-1}^+] \\ &- W_0(m+1)[\alpha^{1/2}N_{m+1}^- - \alpha^{-1/2}N_m^+] \\ &- W_2(m)[\alpha^{1/2}N_{m-1}^- - \alpha^{-1/2}N_m^+] \\ &- W_2(m+1)[\alpha^{1/2}N_m^- - \alpha^{-1/2}N_{m+1}^+]. \end{aligned}$$

We define: $M_m = N_m^- - N_m^+$ and $N_m = N_m^+ + N_m^-$. For thermal equilibrium we define: $M_m = M_e$, $N_m = N_e$, $N_m^+ = N_e^+$, $N_m^- = N_e^-$ and in terms of the Boltzmann factor one may write $N_e^+ = \alpha N_e/(1+\alpha)$, $N_e^- = N_e/(1+\alpha)$. Now assume that the transition $T_1(m)$ has been saturated for such a short time that no nuclear orientation has had time to develop, and, that during the relaxation of the populations we may ignore any transfer of populations out of the nuclear substate $m$, and further, that the populations $N_{m+1}$ and $N_{m-1}$ do not change appreciably from their thermal equilibrium values. Therefore, in the rate equation we set,

$$N_m = N_e, \quad N_{m\pm1}^{\pm} = N_e^{\pm},$$

and obtain after some rearrangement

$$\begin{aligned} dM_m/dt &= -(M_m - M_e)W_1(m)(\alpha^{1/2}+\alpha^{-1/2}) + W_0(m)\alpha^{1/2} \\ &\quad + W_0(m+1)\alpha^{-1/2} + W_2(m)\alpha^{-1/2} + W_2(m+1)\alpha^{1/2}, \\ &= -(M_m - M_e)/\tau_1(m), \end{aligned}$$

which is the first-order result for the apparent relaxation rate $\tau_1(m)$. This apparent relaxation rate will be highly accurate even when $W_0(m)$ and $W_2(m)$ are large if the transition is saturated for a short time in the sense defined above and the initial slope of the recovery is used. In our experiments we were forced to use most of the decay and could not detect any deviation from a pure exponential. It is characteristic of these measurements, that the decay rate can seldom be distinguished from a pure exponential, and the only criterion of validity is that the contributions of $W_0$ and $W_2$ not be much more than 10%.